Preparation and Characterization of Biochar from Four Types of Waste Biomass under Matched Conditions

Yu Hu,[a,#] Pei-yuan Li,[b,#] Yuan-ping Yang,[a] Meng Ling,[a] and Xian-fa Li [a,*]

Four contrasting types of waste biomass were subjected to matching treatments to prepare biochar for the potential removal or immobility Cr(VI) in polluted water or soil. Rice straw (RS), rice husk (RH), kraft lignin (KL), and cow dung (CD) were selected. The resulting biochars were characterized by Fourier transform infrared spectroscopy (FTIR), scanning electron microscopy (SEM), and N_2 adsorption-desorption isotherms. The physicochemical properties of biochars, such as pH value, ash, yield, and cation exchange capacity (CEC) were also determined. The results showed that the biochars were alkaline, except for the KL biochar (KLBC), which was weakly acidic. Furthermore, the order of CEC was cow dung biochar (CDBC) > rice straw biochar (RSBC) > rice husk biochar (RHBC) > KLBC. FTIR showed that there are abundant oxygen-containing functional groups on the surface of the biochars, with the total amount almost the same, and the structure was dominated by aromatic ring skeleton. The KLBC with micro-nano structure exhibited higher surface area (111 m^2/g) than the other BC samples. The Cr(VI) removal followed the order: KLBC > CDBC > RHBC > RSBC.

DOI: 10.15376/biores.17.4.6464-6475

Keywords: Biochar; Waste biomass; Physicochemical properties; Adsorption properties

Contact information: a: School of Life Science and Engineering, Southwest University of Science and Technology, Mianyang 621010, China; b: Institute of Innovation & Entrepreneurship, Southwest University; # These authors contributed equally; Corresponding author: lixianfa@swust.edu.cn*

INTRODUCTION

Biochar is a carbon-rich and stable solid organic material produced through oxygen-limited thermochemical processes from biomass at relatively low temperature (below 700 °C) pyrolytic conditions (Liu *et al.* 2017; Ghodake *et al.* 2021). The unique physical and chemical properties of biochar determine that it exhibits a variety of properties. Biochar has the advantages of high specific surface area and developed pore structure, abundant surface oxygen-containing functional groups, typically high pH value, relatively high cation exchange capacity, and abundant raw materials (Kumar *et al.* 2020; Tomczyk *et al.* 2020). Biochar can enhance soil fertility, improve soil quality, and affect microbial community structure (Dai *et al.* 2021b; Nejad *et al.* 2021; Saffari *et al.* 2021). At the same time, biochar is also beneficial to plant growth and nutrient absorption from soil and improves soil water holding capacity (Dai *et al.* 2021a; He *et al.* 2021; Zhang *et al.* 2021). Biochar can also be used as an adsorbent to remediate heavy metal contaminations in soil and water. Because of stability and carbon enrichment of biochar, it can reduce the emission of CO_2 and N_2O in soil (Woolf *et al.* 2010; Case *et al.* 2015; Qin *et al.* 2020), thus reducing the greenhouse effect.

Chromium has been reported to be one of the most toxic ions to the human body among the heavy metal ions. Chen *et al*. (2022) prepared bagasse pith-derived biochar for high-efficiency removal of Cr(VI) with removal capacity of 185 mg/g and further hydrogenation of furfural. Kokab *et al.* (2021) prepared biochar from walnut shell that was effective for removal of Cr(VI) from wastewater with the maximum removal of 93%. An *et al*. (2022) reported that *Pseudomonas hibiscicola* strain L1 immobilized on peanut shell biochar was used to remove Ni(II), Cr(VI), Cu(II), and nitrate in mix-wastewater. The results illustrated that the removal ratios of Ni(II), Cr(VI), Cu(II) and nitrate were 81.17%, 38.21%, 45.84% and 75.19%, respectively.

However, the application of biochar in different areas depends on its physical and chemical properties. These can be expected to be closely related to raw materials and carbonization conditions, *viz.*, carbonization temperature and pyrolysis time. In general, with the increase of pyrolysis time and carbonization temperature, the ash content and specific surface area will gradually increase, while the cation exchange capacity (CEC) and surface oxygen-containing functional groups will decrease (Sahoo *et al.* 2021; Xie *et al.* 2021). At the same time, raw materials also have a great impact on the properties of biochar, such as the number and types of oxygen-containing functional groups on the surface, which is an important factor in determining the final application and effect of biochar (Rodriguez *et al.* 2020). Wang *et al.* (2018) investigated the adsorption behavior of different raw materials on Cd^{2+} on biochar and its relative adsorption mechanism. They found that due to the different composition of raw materials and oxygen-containing functional groups, the role of the involved Cd^{2+} removal mechanism varies with different raw materials.

Although different pyrolysis conditions directly affect the yield, and physical and chemical properties of biochar, even if the pyrolysis conditions are the same, the differences in properties of biochar prepared from various raw materials also limit its application in soil improvement, heavy metal pollution remediation, and other fields (Guo *et al.* 2021). Therefore, in this study, four different biomass materials were selected to prepare biochar under the same carbonization conditions. The variances in physical and chemical properties of the prepared biochar from different raw materials were investigated, and on this basis, the adsorption performances of the four biochars for Cr(VI) adsorption was studied, which provided a reference for the selection of stable adsorbents for heavy metal pollution control.

EXPERIMENTAL

Materials

A muffle furnace, SX-5-12 from Tianjin Tester Instrument Co., Ltd. (Tianjin, China) and a WFJ7200 Spectrophotometer from Shanghai Unico Instrument Co., Ltd. (Shanghai, China) were used.

Rice straw (RS) and rice husk (RH) were collected at the Experimental Farm of Southwest University of Science and Technology located at Mianyang, China; cow dung (CD) was purchased online (collected at Dabie Mountain, Jinzhai County, Anhui, China); kraft lignin (KL) from papermaking wastewater was purchased from Shandong Xuemei Paper Co., Ltd. (Shandong, China). Sulfuric acid (H_2SO_4), hydrochloric acid (HCl), sodium hydroxide (NaOH), barium chloride ($BaCl_2$), and potassium dichromate ($K_2Cr_2O_7$) used were analytically pure and purchased from Chengdu Cologne Chemicals Co., Ltd. (Sichuan, China).

Biochars preparation

The preparation of the biochars was as in the method described by Hu *et al.* (2021). The raw material samples RS, RH, CD, and KL were pyrolyzed in the muffle furnace at 400 °C for 2 h and then cooled to room temperature. The pyrolyzed samples were then washed with distilled water to remove the soluble impurities to obtain biochars. The biochar samples were labeled based on different raw materials, bagged, sealed, and stored in a dry place for later use.

Methods

Characterization of biochars

The specific surface area and pore size distribution of the biochars were measured by nitrogen adsorption using an Autosorb-1MP analyzer (Konta, USA). The samples were degassed in vacuum at 350 K for 6 h before testing. The surface morphology of the biochars was examined by scanning electron microscopy (SEM) (Carl Zeiss NTS GmbH, UItra55, Germany).

The surface functional groups in the biochars were determined by Fourier transform infrared spectroscopy (FT-IR) (PE, Spectrum One, USA); the pH value of the biochars (solid-liquid ratio 1:20) was determined by a pH meter; the ash content was determined using charcoal and charcoal standard (GB/T17664-1999). CEC was determined by barium chloride-sulfuric acid method.

Bath adsorption experiments

A Cr(VI) stock solution (1000 mg/L) was prepared with ultrapure water and $K_2Cr_2O_7$, and the pH was adjusted to 5 with 1.0 mol/L HCl and NaOH solutions. About 0.2 g of biochar was accurately weighed and placed in a 150 mL conical flask containing the above solution (50 mL, 50 mg/L). Vibration adsorption was performed at 150 rpm in a constant-temperature water bath at 25±1 °C for 24 h, and the suspension after adsorption was subjected to vacuum filtration using a 0.45 μm aqueous filter membrane. The concentration of Cr(VI) was determined *via* diphenylcarbonyl dihydrazine spectrophotometry (Wang *et al.* 2019) (WFJ7200 spectrophotometer, Shanghai). The elimination % of Cr(VI) solution can be calculated by Eq. 1,

$$Removal\ \% = \frac{(c_0 - c_t)}{c_0} \times 100 \quad (1)$$

where c_0 is the initial mass concentration of Cr(VI) in the solution (mg/L) and c_t is the mass concentration of Cr(VI) in the solution (mg/L) at time t (h).

.

Statistical analysis

Data were analyzed by one-way analysis of variance and Least Significant Difference (LSD) tests to compare means of three replicates. Differences were considered significant at $p < 0.05$.

RESULTS AND DISCUSSION

Yield, Ash, pH, and CEC of Biochars from Different Raw Materials

As shown in Table 1, by comparing the yields of biochar, the following order KLBC > RHBC > RSBC > CDBC was obtained, which can be mainly attributed to the

nature of raw materials. The RS and RH samples contained a lot of cellulose and hemicellulose, and the molecular weights of cellulose and hemicellulose are lower than that of lignin. When the temperature rises to 400 °C and above, it is easier to crack and release these in the form of gas, while lignin has strong thermal stability and it exhibits less mass loss. It was found that the ash contents of RSBC, RHBC, and CDBC were similar, which may be caused by the degradation and mineralization of cellulose volatile substances contained in raw materials during pyrolysis (Tsai *et al.* 2012). As a soil amendment, the influence of pH of biochar on the physical and chemical properties of soil cannot be ignored. The pH value of the biochar varies because of the different characteristics of the raw materials. By comparing the pH values of different raw materials, it was found that the pH values of biochar were all alkaline except that of KLBC. The order of pH value was RHBC > RSBC > CDBC > KLBC. Based on these findings, the first three kinds of biochars were judged to be suitable for improving acidic soil.

Table 1. Physical and Chemical Properties of Biochars

Biochars	Yield (%)	pH	Ash (%)	CEC per cmol/kg
CDBC	36.57	8.30	37.68	141.41
RSBC	37.82	9.82	35.34	23.83
RHBC	43.83	10.07	36.76	6.96
KLBC	59.40	4.81	8.78	4.48

CEC is usually used to measure the ability of soil to retain nutrients, and its value determines the effect of biochar on soil cation exchange. The higher CEC value of the biochar indicates greater the ion exchange capacity of the soil. Thereby the nutrient retention capacity of the soil was enhanced. Comparing the CEC of different biochar materials, it was found that the order was CDBC > RSBC > RHBC > KLBC.

Elemental Composition of Biochar

The elemental composition of the biochar from various raw materials is shown in Table 2. The raw material of the biochar determines the elemental compositions of the resulting biochar. The aromaticity, polarity, and hydrophilicity of a substance can be expressed in terms of H/C, (N+O)/C, and O/C atomic ratios, respectively (Binda *et al.* 2020). The aromatization degree of KLBC is the highest, which reveals its stable structure. CDBC has high polarity and hydrophilicity and contains more oxygen-containing functional groups.

Table 2. Element Composition of Biochars

Biochars	C (%)	H (%)	N (%)	O (%)	H/C	O/C	(O+N)/C
CDBC	40.66	2.16	2.09	17.34	0.053	0.427	0.478
RSBC	47.31	2.12	0.62	14.33	0.045	0.303	0.316
RHBC	50.98	2.32	1.85	6.66	0.046	0.131	0.167
KLBC	68.05	2.45	1.45	19.28	0.036	0.283	0.305

SEM Analysis

The SEM images of biochars prepared from different raw materials are shown in Fig. 1. The biochars prepared from RS, RH, and CD had obvious pore structure, but the size and number of pores were different. After pyrolysis and carbonization, the structure

of biochar was destroyed, and some pores with various shapes appeared. Among these RSBC, RHBC, and CDBC had abundant pore structures, which were honeycomb-shaped and closely arranged. However, the surface structure of KLBC was compact, and the number of pores was less. This may have been due to the collapse of the pore structure with the increase of temperature, resulting in small and dense pores. Comparing with the precursor feedstock, KL and KLBC had irregular grain structure. No obvious pore structure was found on the KL surface.

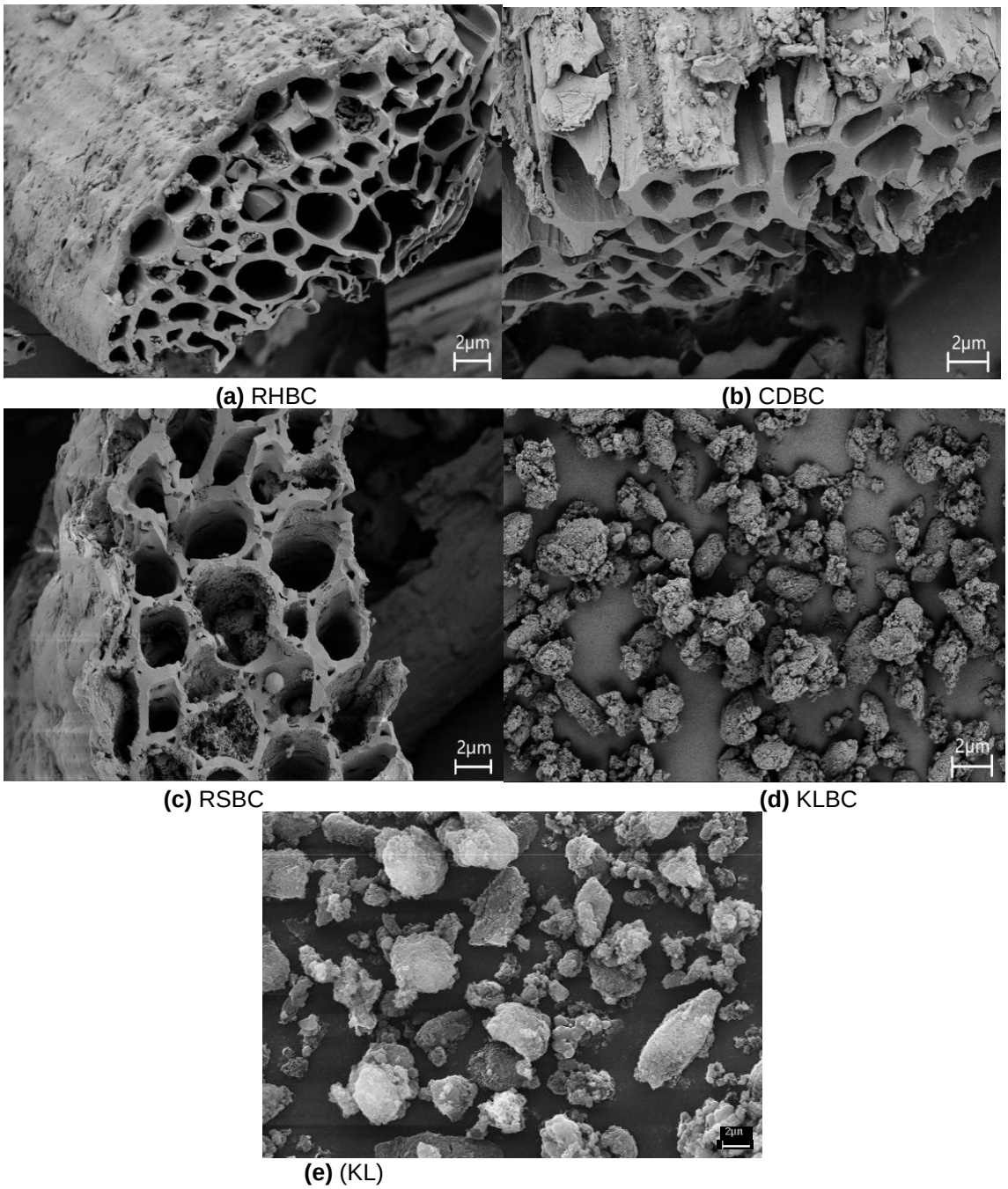

(a) RHBC **(b)** CDBC

(c) RSBC **(d)** KLBC

(e) (KL)

Fig. 1. SEM images of biochars from different raw materials (2 kx) and feedstock KL (10kx)

Specific Surface Area and Pore Size of Biochars

The specific surface area, pore volume, and pore size of biochar varied considerably with different raw materials. The specific surface area of biochar was mainly determined by the presence of micropores. Among them, the specific surface area of RHBC was the smallest, which may be attributable to a large amount of ash filling or blocking the micropores during the carbonization process (Lapham and Lapham 2019). This is consistent with the SEM observation results. RHBC had more macropores, so the specific surface area was smaller, while KLBC may contain abundant meso- and micro-pores in its structure, so the specific surface area was larger, up to 111.2 m^2/g.

Figure 2 shows that the adsorption and desorption isotherms of these four biochars were separated with decreasing P/P_0. This finding is consistent with a type IV isotherm according to the IUPAC classification. The hysteresis loop belongs to type H, and the adsorption-desorption hysteresis phenomenon is related to the shape and size of pores (Kondo *et al.* 2005). As can be seen in the figure, the hysteresis loops of adsorption-desorption isotherms of CDBC, RSBC, and KLBC in the range of $P/P_0 < 0.1$ are not closed. Such results can be expected when most of the holes of char materials are flexible pores or ink bottle holes, and the diameter of the pores shrinks after gas adsorption. As a result, the adsorbed gas is not as easy to desorb. A further reason for a hysteresis loop not to close is when there is strong adsorption induced by a microporous structure inside the biochar. RHBC did not show any adsorption limitation in the higher relative pressure region, indicating the presence of macropores within the RHBC, which is consistent with SEM observations.

The textural characteristics of biochars prepared from various feedstock and KL are shown in Table 3. The surface area of four biochars followed the order KLBC > RSBC > CDBC > RHBC. After carbonization of KL, the specific surface area and total pore volume increased from 27.1 m^2/g and 0.08 cm^3/g to 111.2 m^2/g and 0.19 cm^2/g, respectively, indicating that abundant meso- and macro-pores were formed during carbonization.

Table 3. Comparison of the Textural Characteristics of KL and Biochars

Sample	A_{BET} (m^2/g)	V_t (cm^3/g)	D (nm)
RHBC	4.1	0.02	236
CDBC	27.0	0.05	79
RSBC	30.3	0.03	45
KLBC	111.2	0.19	69
KL	27.1	0.08	18

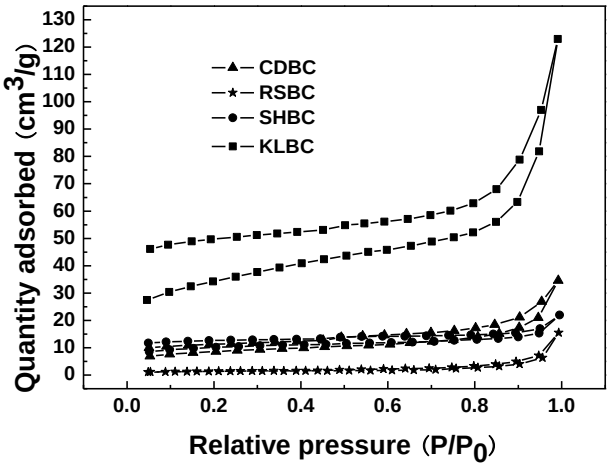

Fig. 2. N_2 adsorption-desorption isotherms of biochar prepared from different raw materials

According to IUPAC definition, the pore size range of 2 nm to 50 nm is mesopores, and more than 50 nm is macropores. The pore size distribution curve is shown in Fig. 3. It can be seen that the surface areas of meso- and macro-pores of CDBC, RSBC, and RHBC were small. However, the surface areas of meso- and macro-pores of KLBC was large, resulting in large total surface area (111.2 m^2/g) and pore volume of KLBC. In addition, the micro- and nano structure features of KLBC increased its surface area.

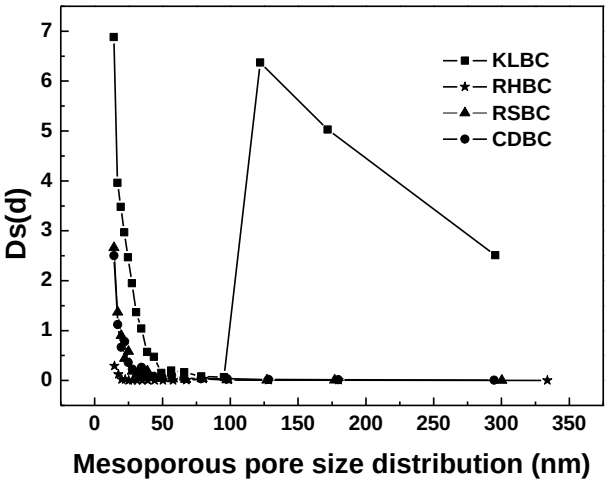

Fig. 3. Pore size distribution of biochar prepared from different raw materials

FT-IR Analysis

The FT-IR analysis is an effective tool to observe the changes of oxygen-containing functional groups on the surface of biochar. It can be seen from Fig. 4 that the characteristic absorption peaks of the four kinds of biochars were roughly the same, indicating that the types of functional groups contained were fundamentally the same.

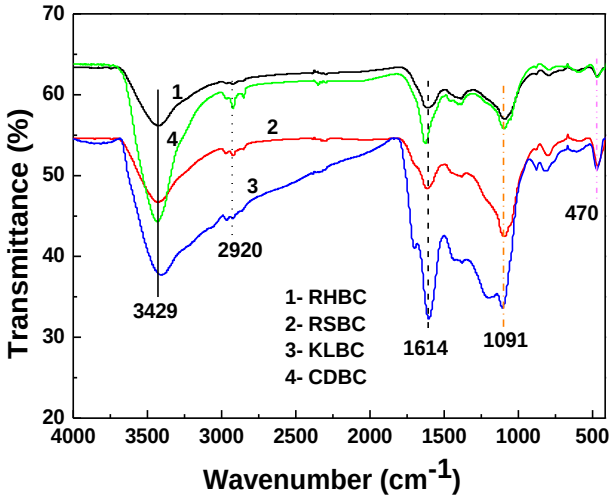

Fig. 4. The FT-IR of biochars prepared from different raw materials

The peak at 3429 cm^{-1}, indicates mainly the stretching vibration of -OH, and that at 2920 cm^{-1} was the C-H (methyl-CH_3, methylene-CH_2) vibration in alkanes. The peaks at 1614 cm^{-1} were the stretching vibration of C=C on the aromatic ring, at 1091 cm^{-1} was the symmetric stretching vibration of -C-O-C, at 800 cm^{-1} was the out-of-plane bending vibration of C-H on the benzene ring, and at 470 cm^{-1} was Si-O vibration. These results showed that there were abundant hydroxyl, carboxyl, and carbonyl functional groups on the surface of biochars, and its main structure was comprised of aromatic ring skeleton.

Comparison of Adsorption Performances of Biochar

Cr(VI) adsorption tests were carried out using the prepared biochars from different biomass raw materials, and the results are shown in Fig. 5. It can be seen that the adsorption performance of biochar was obviously different, and the removal efficiency for Cr(VI) ion of KLBC was higher than that of CDBC, RHBC, and RSBC. This may be related to the high specific surface area and surface oxygen-containing functional groups of KLBC. The developed pore structure and large specific surface area of KLBC provided a large number of effective adsorption sites for the heavy metal ions. The surface of biochar contains carboxyl, hydroxyl, and other oxygen-containing functional groups, which form stable complexes with Cr(VI) ions on the surface, which is more conducive to the adsorption of chromium ions.

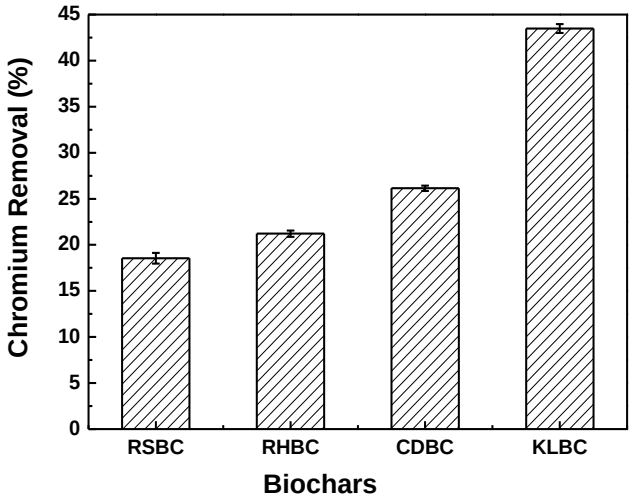

Fig. 5. Effect of biochars prepared from different raw materials on Cr(VI) removal. The error bars represent the standard deviation (n = 3)

CONCLUSIONS

Biochar derived from various feedstock showed different properties of surface area, porosity, and morphology.

1. Under the same carbonization conditions, the yield and carbon content of the four biochars followed the order KLBC > RHBC > RSBC > CDBC, while CEC showed the opposite result. RHBC, RSBC and CDBC were weakly alkaline and had higher ash content, ranging from 35.34% to 37.68%; KLBC was acidic with low ash content (8.78%).
2. The surface morphology of RHBC, RSBC, and CDBC was a mesh-like structure, but the surface area was small; KLBC was irregular micro-nano particles and had abundant microporous and mesoporous structure, with a high specific surface area (111.2 m^2/g).
3. The results of FT-IR characterization showed that there were abundant oxygen-containing functional groups on the surfaces of the four biochars, which were beneficial to the adsorption of Cr(VI), and the structure of the four biochars was mainly comprised of aromatic ring skeleton, which had good stability.
4. The removal of Cr(VI) by the four biochars followed the order RSBC < RHBC < CDBC < KLBC, which was positively correlated with surface area and pore structure.

REFERENCES CITED

An, Q., Jin, N., Deng, S., Zhao, B., Liu, M., Ran, B., and Zhang, L. (2022). "Ni(II), Cr(VI), Cu(II) and nitrate removal by the co-system of *Pseudomonas hibiscicola* strain L1 immobilized on peanut shell biochar," *Science of the Total Environment* 814, 152635. DOI: 10.1016/j.scitotenv.2021.152635

Binda, G., Spanu, D., Bettinetti, R., Magagnin, L., Pozzi, A. A., and Dossi, C. (2020). "Comprehensive comparison of microalgae-derived biochar from different feedstocks: A prospective study for future environmental applications," *Algal Research* 52, article no. 102103. DOI: 10.1016/j.algal.2020.102103

Case, S. D, McNamara, N. P., Reay, D. S., Stott, A. W., Grant, H. K., Whitaker, J., and Lancaster, E. C. (2015). "Biochar suppresses N_2O emissions while maintaining n availability in a sandy loam soil," *Soil Biology and Biochemistry* 81, 178-185. DOI: 10.1016/j.soilbio.2014.11.012

Chen, D., Chen, S., He, L., Guan, Q., Miao, R. (2022). "Preparation of bagasse pith-derived biochar for high-efficiency removal of Cr(VI) and further hydrogenation of furfural," *Biomass Conversion and Biorefinery*. DOI: 10.1007/s13399-022-02547-5

Dai, W., Xu, M., Zhao, Z., Zheng, J., Huang, F., Wang, H., Liu, C., and Xiao, R. (2021a). "Characteristics and quantification of mechanisms of Cd^{2+} adsorption by biochars derived from three different plant-based biomass," *Arabian Journal of Chemistry* 14(5). DOI: 10.1016/j.arabjc.2021.103119

Dai, Z., Xiong. X., Zhu, H., Xu, H., Leng, P., Li, J., Tang, C., and Xu, J. (2021b). "Association of biochar properties with changes in soil bacterial, fungal and fauna communities and nutrient cycling processes," *Biochar* 3(3), 239-254. DOI: 10.1007/s42773-021-00099-x

Ghodake, G. S., Shinde, S. K., Kadam, A. A., Saratale, R. G., Saratale, G. D., Kumar, M., Palem, R. R., AL-Shwaiman, H. A., Elogorban, A. M., Syed, A., Kim, D. Y., and Dongguk, U. S. (2021). "Review on biomass feedstocks, pyrolysis mechanism and physicochemical properties of biochar: State-of-the-art framework to speed up vision of circular bioeconomy," *Journal of Cleaner Production* 297(16), article no. 126645. DOI: 10.1016/j.jclepro.2021.126645

Guo, J., Zheng, L., Li, Z., Zhou, X., Cheng, S., and Zhang, L. (2021). "Effects of various pyrolysis conditions and feedstock compositions on the physicochemical characteristics of cow manure-derived biochar," *Journal of Cleaner Production* 311(3), 127458. DOI: 10.1016/j.jclepro.2021.127458

He, M., Xiong, X., Wang, L., Hou, D., Bolan, N. S., Ok, Y. S., Rinklebe, J. T., and Daniel, C. W. (2021). "A critical review on performance indicators for evaluating soil biota and soil health of biochar-amended soils," *Journal of Hazardous Materials* 414(20), article no. 125378. DOI: 10.1016/j.jhazmat.2021.125378

Hu, Y., Ling, M., Li, X. F. (2021). "Preparation of lignin-based mesoporous biochar nano-, microparticles, and their adsorption properties for hexavalent chromium," *BioResources* 16(3), article no. 6363. DOI: 10.15376/biores.16.3.6363-6377.

Kondo, S., Ishikawa, T., and Abe, I. (2005). "Absorption isotherms," in: *Adsorption Science*, F. Y. Liu (ed.), Chemical Industry Press, Beijing, China, pp. 31-103.

Kokab, T., Ashraf, H. S., Shakoor, M. B., Jilani, A., Ahmad, S. R., Majid, M., Ali, S., Farid, N., Alghamdi, R. A., Al-Quwaie, D. A. H., and Hakeem, K. R. (2021). "Effective removal of Cr(VI) from wastewater using biochar derived from walnut

shell," *International Journal of Environmental Research and Public Health* 18, article no. 9670. DOI: 10.3390/ijerph18189670

Kumar, A., Saini, K., and Bhaskar, T. (2020). "Hydochar and biochar: Production, physicochemical properties and techno-economic analysis," *Bioresource Technology* 310, article no. 123442. DOI: 10.1016/j.biortech.2020.123442

Lapham, D. P., and Lapham, J. L. (2019). "BET surface area measurement of commercial magnesium stearate by krypton adsorption in preference to nitrogen adsorption," *International Journal of Pharmaceutics* 568, article no. 118522. DOI: 10.1016/j.ijpharm.2019.118522

Liu, Y., Yao, S., Wang, Y., Lu, H., Brar, S. K., and Yang, S. (2017). "Bio- and hydrochars from rice straw and pig manure: Inter-comparison," *Bioresource Technology* 235, 332-337. DOI: 10.1016/j.biortech.2017.03.103

Nejad, Z. D., Rezania, S., Jung, M. C., AI-Ghamdi, A. A., Mustafa, A. E., Elshikh, M. S., and Sejong, U. (2021). "Effects of fine fractions of soil organic, semi-organic, and inorganic amendments on the mitigation of heavy metal(loid)s leaching and bioavailability in a post-mining area," *Chemosphere* 271, article no. 129538. DOI: 10.1016/j.chemosphere.2021.129538

Qin, X. X., Luo, J. X., and Liu, Z. G. (2020). "Preparation and characterization of MgO-modified rice straw biochars," *Molecules* 25(23), article no. 5730. DOI: 10.3390/molecules25235730

Rodriguez, J. A., Filho, J., Melo, L., Assis, L., and Oliveira, T. (2020). "Influence of pyrolysis temperature and feedstock on the properties of biochars produced from agricultural and industrial wastes," *Journal of Analytical and Applied Pyrolysis* 149, article no. 104839. DOI: 10.1016/j.jaap.2020.104839

Saffari, N., Hajabbasi, M. A., Shirani, H., and Mosaddeghi, M. R. (2021). "Influence of corn residue biochar on water retention and penetration resistance in a calcareous sandy loam soil," *Geoderma* 114734. DOI: 10.1016/j.geoderma.2020.114734

Sahoo, S. S., Vijay, V. K., Chandra, R., and Kumar, H. (2021). "Production and characterization of biochar produced from slow pyrolysis of pigeon pea stalk and bamboo," *Cleaner Engineering and Technology* 3, article no. 100101. DOI: 10.1016/j.clet.2021.100101

Tomczyk, A., Sokołowska, Z., Boguta, P., and Polish, A. S. (2020). "Biochar physicochemical properties: pyrolysis temperature and feedstock kind effects," *Reviews in Environmental Science and Bio/Technology* 19, 191-215. DOI: 10.1007/s11157-020-09523-3

Tsai, W. T., Liu, S. C., Chen, H. R., Chang, Y. M., and Tsai, Y. L. (2012). "Textural and chemical properties of swine-manure-derived biochar pertinent to its potential use as a soil amendment," *Chemosphere* 89, 198-203. DOI: 10.1016/j.chemosphere.2012.05.085

Wang, R. Z., Huang, D. L., Liu, Y. G., Zhang, C., Lai, C., Zeng, G. M., Cheng, M., Gong, X. M., Wan, J., and Lou, H. (2018). "Investigating the adsorption behavior and the relative distribution of Cd^{2+} sorption mechanisms on biochars by different feedstock," *Bioresource Technology* 261, 265-271. DOI: 10.1016/j.biortech.2018.04.032

Wang, H. X., Zhang, M. L., and Lv, Q. (2019). "Removal efficiency and mechanism of Cr(VI) from aqueous solution by maize straw biochars derived at different pyrolysis temperatures," *Water* 11(4), 781. DOI: 10.3390/w11040781

Woolf, D., Amonette, J. E., Street-perrott, F. A., Lehmann, J., and Joseph, S. (2010). "Sustainable biochar to mitigate global climate change," *Nature Communications* 1(5), 56. DOI: 10.1038/ncomms1053

Xie, R., Zhu, Y., Zhang, H., Zhang, P., and Han, L. (2021). "Effects and mechanism of pyrolysis temperature on physicochemical properties of corn stalk pellet biochar based on combined characterization approach of microcomputed tomography and chemical analysis," *Bioresource Technology* 329, article no. 124907. DOI: 10.1016/j.biortech.2021.124907

Zhang, Y., Wang, J., and Feng, Y. (2021). "The effects of biochar addition on soil physicochemical properties: A review," *Catena* 202(2), article no. 105284. DOI: 10.1016/j.catena.2021.105284

Article submitted: April 9, 2022; Peer review completed: May 14, 2022; Revised version received: May 31, 2022; Accepted: June 1, 2022; Published: October 3, 2022.
DOI: 10.15376/biores.17.4.6464-6475